ACS Biomaterials SCIENCE & ENGINEERING
Cite This: ACS Biomater. Sci. Eng. 2020, 6, 2652−2658
Article
pubs.acs.org/journal/abseba

Injectable Flexible Subcutaneous Electrode Array Technology for Electrocardiogram Monitoring Device

Jihye Bong,[†] Omar Yasin,[‡] Vaibhav R. Vaidya,[‡] Jeongpil Park,[†] Zachi I. Attia,[‡] Deepak Padmanabhan,[‡] Sang June Cho,[†] Roshini Asirvatham,[‡] Noah Schneider,[‡] Juhwan Lee,[†] Eun Mee Kim,[§] Paul A. Friedman,*[,‡] and Zhenqiang Ma*[,†]

[†]Department of Electrical and Computer Engineering, University of Wisconsin−Madison, Madison, Wisconsin 53706, United States
[‡]Department of Cardiovascular Diseases, Mayo Clinic, Rochester, Minnesota 55905, United States
[§]Department of Emergency Medical Technology, Korea Nazarene University, Cheonan 31172, South Korea

Supporting Information

ABSTRACT: Implantable cardiac monitors have undergone considerable miniaturization. However, they continue to be associated with complications such as infection, bleeding/bruising, and device extrusion or migration. In this paper, we demonstrate the feasibility of using a small, flexible, injectable, subcutaneous microelectrode-based device to record electrocardiograms (ECGs). We describe the fabrication process and demonstrate the ease of insertion of the injectable ECG device in vivo swine model. We also demonstrate our device's high-density channel microelectrode array's ability to detect the P, R, and T waves. The amplitude of these waves showed excellent correlation with distance of the bipolar electrodes used to detect them. Given the success of our initial studies, this device has the potential to improve the safety profile of implantable cardiac monitors and simplify the implantation procedure to allow for placement in a primary care setting.

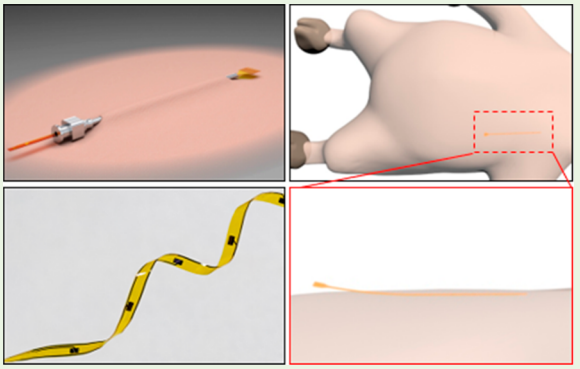

KEYWORDS: *injectable device, flexible electronics, medical implantable monitors, subcutaneous biosensor*

1. INTRODUCTION

Sudden cardiac death (SCD) continues to be the leading cause of mortality in the world.[1] Cardiac rhythm disturbances, such as ventricular arrhythmias, are implicated in the pathophysiology of SCD regardless of the initial precipitating disease process.[1] Arrhythmias are also implicated in the pathophysiology of several disorders including stroke, syncope, and presyncope.[2,3] Even some of the "benign" rhythm disturbances can leave patients with debilitating symptoms and decrease their quality of life.[4]

Lifesaving interventions are available, and if implemented in a timely manner, they can reduce mortality and morbidity associated with cardiac arrhythmias. Given the high disease burden and potential benefits from early detection, practice guidelines recommend the use of ambulatory electrocardiography (ECG) monitoring for detection of arrhythmias.[5,6] Ambulatory ECG monitoring has proven its role in detection of physiologic and pathologic changes in the cardiac rhythm.[7] Surface ECG devices are available for short-term monitoring in the order of days to weeks.

However, the sporadic nature of some of these arrhythmias, and sometimes lack of symptoms, can make diagnosis elusive, thus leaving patients at risk of having their first presenting symptom be a catastrophic event.[1] For example, when monitored long term, 21% of patients with "cryptogenic" stroke were found to have atrial fibrillation which is a known risk factor that can be mitigated with anticoagulation.[3] Monitoring for longer durations is desirable for the diagnosis of infrequent arrhythmias, and can also be useful for long-term assessment of response to therapies.[8] Recent advances in flexible cardiograms have enabled the development of long-term wearable devices and implantable devices.[9−13] Particularly, the subcutaneously implanted cardiac monitors are able to detect various arrhythmias including brady- and tachyarrhythmias, atrial fibrillation, and ischemia.[5,14,15] Implantable cardiac monitors have undergone considerable miniaturization and can now be placed under local anesthesia and with small incisions. While effective, placement of these monitors is not without risk and can be associated with infection in up to 12% of patients.[16] They can also be associated with bleeding/bruising at the implant site and device extrusion or migration can also occur.[16,17] Thus, there is a need to improve the safety

Special Issue: Leaders in Biomedical Engineering

Received: July 22, 2019
Accepted: October 26, 2019
Published: October 26, 2019

DOI: 10.1021/acsbiomaterials.9b01102
ACS Biomater. Sci. Eng. 2020, 6, 2652−2658

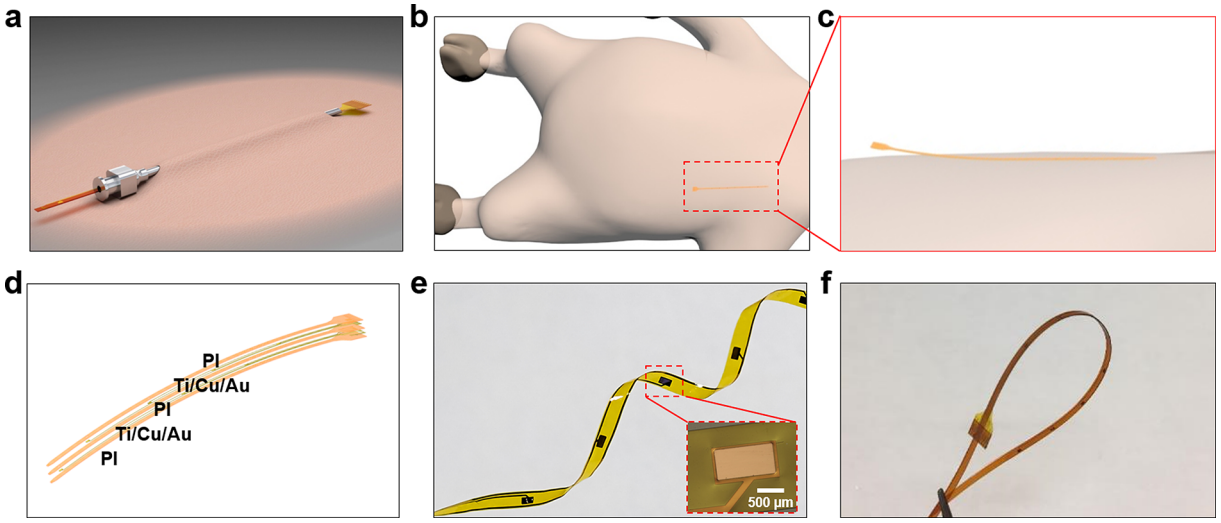

Figure 1. Schematic illustrations and optical images of the flexible subcutaneous injectable electrocardiogram device. (a) Schematic illustration of the subcutaneous injection of a flexible device with a 13-gauge needle. Scheme of implanted I-ECG device in the precordial subcutaneous space of a swine model: (b) top and (c) side view. (d) Diagram of ECG device construction showing the layered structures. (e) Demonstration of device flexibility and the expanded electrode area (inset). (f) Attached I-ECG to rigid carrier PI Kapton film with PVA shows flexibility and steadiness.

and availability of these monitors to improve patient outcomes with a minimally invasive delivery method.[18]

In this project, we aim to further miniaturize the implanted recording electrodes to allow for simpler and less invasive placement procedures and thereby decrease the risk of complications. We also aim to improve current technology by using an array of multiple electrodes and optimizing the interelectrode distance to better categorize the morphology of detected ECG signals. To achieve this, we conducted a prospective proof of concept study to demonstrate the feasibility of developing and using a subcutaneous, injectable, multielectrode ECG device for ECG detection. We hypothesize that such a device (1) can be easily implanted through a needle, and (2) is able to detect ECG signals in sinus rhythm and during simulated and nonsimulated cardiac arrhythmias in vivo swine model.

2. MATERIALS AND METHODS

2.1. Device Fabrication. We envisioned a thin and flexible multielectrode device that can be implanted subcutaneously by injecting it through a needle (Figure 1a–c). The injectable electrocardiogram (I-ECG) device was fabricated using a multilayered structure designed with a Si wafer to hold the substrate (Figure S1). A thin poly(methyl methacrylate) (950 PMMA A2, Microchem) was spin coated as a sacrificial layer and soft baked at 180 °C in air for 3 min. We selected a polyimide (PI, PI-2545, HD MicroSystems) that was spin coated two times at 2500 rpm for 60 s (thickness ∼5 μm) on the surface as a substrate base layer, soft baked at 150 °C for 4 min, and then hard baked at 350 °C under N_2 (4 Torr) ambient for 3 h. Metal Ti (10 nm)/Cu (440 nm)/Au (50 nm) were deposited with a liftoff method as electrodes, traces, and metal pads. The second PI layer was coated with 5 μm thickness again as an insulator between the first and second metal layer. The second metal layer was then deposited. The third PI layer was spin coated as an encapsulated layer of the whole array device. After the electrodes, pads, and array outlines were dry etched with reactive ion etching (RIE), Al was used as a robust mask. The mask was wet etched with AZ-400 K developer (AZ Electronic Materials). Finally, the sacrificial layer PMMA between the Si wafer and PI layers was dissolved in acetone, and the I-ECG device was released from the wafer. The device comprised a high-density, seven-channel active microelectrode array with a length, width, and thickness of 84 mm, 1.24 mm, and ∼15 μm, respectively (Figure 1d and Figure S2). The surface area of each electrode was 0.8 × 0.4 mm^2 and the center-to-center distance between the near electrodes was 8.5 mm (Figure 1e).

Because the subcutaneous I-ECG device is thin, soft, and long, a rigid carrier PI Kapton film (thickness 500 μm) was used to make device handling and placement easier (Figure 1f). The device was attached to the carrier with poly(vinyl alcohol) (PVA, Sigma-Aldrich), which is commonly used as a biomaterial because it is biocompatible, nontoxic, noncarcinogenic, highly water soluble, and bioadhesive in medical devices (Figure S3a–c).[19] PVA has a carbon–carbon single-bond backbone that is fully biodegradable.[20] In addition, the hydroxyl (–OH) groups on alternating carbon atoms are polar and therefore water soluble, and thus PVA is hydrophilic, which also promotes its degradation through hydrolysis.

2.2. Electrochemical Measurement. A three-electrode system was used with Au-based ECG as the working electrode (WE), the platinum as the counter electrode (CE), and Ag/AgCl as the reference electrode (RE) in saline (0.9% w/v NaCl) solution and in the atmosphere. The seven-channel Au-based electrode was connected to the Autolab PGSTAT 128N (Metrohm Autolab, Netherlands) via a ZIF (Zero Insertion Force) PCB (Printed Circuit Board) connector. For the electrochemical impedance spectroscopy (EIS), 50 mV sine waves at frequencies from 0.1 to 100 kHz were used. To mimic the biofluidic environment, the device was tested while submerged in normal saline solution (0.9% w/v solution).

2.3. Animal Preparation. In vivo testing of the I-ECG device was conducted at Mayo Clinic's Cardiovascular Innovation Laboratory. All procedures were reviewed and approved by the Mayo Clinic Institutional Animal Care and Use Committee. A female swine model (*Sus Scorfa*) was used for the experiments. Animals were fasted overnight. Intramuscular Telazol (5 mg/kg) and Xylazine (2 mg/kg) were used for anesthesia induction after which the animals underwent endotracheal intubation. Animals were placed in the supine position on the operating table. Isoflurane (1–3%) inhalation was used to maintain anesthesia. Continuous pulse oximetry was used for monitoring and supplemental oxygen utilized as needed. Core body temperature was maintained around 38 °C using a heating pad. The anterior chest wall and femoral regions were shaved and prepped for vascular access and device placement. The femoral artery was used for continuous blood pressure monitoring and femoral vein was used for venous access. Standard ECG clips were also placed to obtain surface ECG and connected to a general electric Prucka system. Cefazolin (40 mg/kg, intravenous) was administered in all animals.

DOI: 10.1021/acsbiomaterials.9b01102
ACS Biomater. Sci. Eng. 2020, 6, 2652–2658

2.4. Device Placement. Fluoroscopy was used to determine the location and orientation of the heart in an anterior-posterior view while in supine position. Movie S1 shows the operation of the implantation process. A 13-gauge needle (outside diameter: 2.41 mm) was placed on the animal's chest overlying the heart and fluoroscopy was used to determine the optimal position and orientation of the needle so that it lays over the myocardium. Once determined, a small (0.5 cm) superficial incision was made through the cutaneous layer at the needle entrance site to avoid excessive tugging. Through the incision, the 13-guage needle was tunneled in the subcutaneous layer (Figure 2a). The tip of the needle was exteriorized at a predetermined location (Figure 2a). The I-ECG device (mounted on the carrier PI) was then gently fed into the lumen of the needle through its distal tip and advanced using small pickups (Figure 2b). Once the device was fully in position, the needle was retracted slowly while traction was simultaneously applied at the proximal end of the device. With this technique, the needle was fully removed and the device remained in the subcutaneous layer within the tunneled tract created by the needle (Figure 2c). The device's position was confirmed using fluoroscopy. Finally, the PVA between the subcutaneous ECG electrodes and the carrier PI was allowed to dissolve in subcutaneous extracellular fluid for a few minutes and the carrier PI was gently removed by simple traction (Figure 2d). The header of I-ECG device was the only portion of the device that remained externalized to be connected for data collection using the CardioLab (GE Medical Systems Information Medical Technologies, Inc.) signal acquisition system.

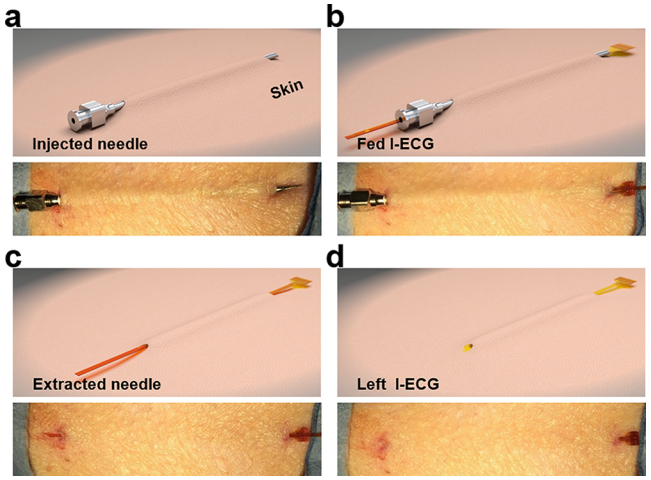

Figure 2. Schematic illustration (top) and optical images (bottom) of a novel inserted subcutaneous ECG process with a needle in the subcutaneous space of a swine under anesthesia. (a) Injection with a 13-gauge needle (outer diameter: 2.41 mm) under the skin. (b) I-ECG device feeds into place through the lumen. (c) Gentle extraction of the needle. (d) After the carrier PI was removed by simple traction, the I-ECG device is left in place.

2.5. Data Acquisition and Processing. The entire procedure was recorded using the CardioLab system. All signals were filtered at 0.05−150 Hz with a 60 Hz notch filter. At times, filter settings were changed to assess for changes in ECG and eliminate respiratory drift. The proximal most electrode on our subcutaneous I-ECG device was used as a reference electrode for bipolar signal acquisition between it and one of the other electrodes on the same device. Therefore, six pairs of bipolar electrograms were expected from each device based on a seven-channel device. The Wilson's central terminal was used for unipolar ECG acquisition. For comparison, standard surface electrodes were used to simultaneously record the surface ECG. Data were then reviewed retrospectively on the CardioLab system where different measurements were manually obtained for the different waves and segments. Means and standard deviation for all analyzed signals from surface ECG were reported using Microsoft Excel Version 14.0.7232.5000 (Part of Microsoft Office Standard 2010). Correlation coefficients and Bland-Altman plots were generated using MedCalc Statistical Software version 18.11.3 (MedCalc Software bvba, Ostend, Belgium; https://www.medcalc.org; 2019).

2.6. Simulated Arrhythmias. A 7 French Blazer catheter was advanced to the right atrium through the femoral vein access. Burst pacing at various cycle lengths and atrial extra stimulus testing was performed to assess fidelity of the recorded signals at various rates and with pacing artifact. The catheter was then advanced to the right ventricle and similar testing was performed. Some ectopy was also recorded from manual catheter manipulation within the heart. Once data was collected, if the plan was to keep the animal alive for a future procedure then femoral access sheaths were withdrawn and manual pressure was applied for hemostasis. The devices were extracted from the subcutaneous space using simple traction. If the plan was to sacrifice the animal (for final experiment), ventricular fibrillation was induced by direct current application at the end of the procedure.

3. RESULTS AND DISCUSSION

3.1. Electrochemical Characterization. Electrochemical impedance was used to probe the ion diffusion and electron charge transfer and to understand the electrochemical performance in recording electrode−electrolyte interface.[21] To investigate the interface impedance property of the Au-based ECG, the Au electrodes with area of 800 × 400 μm^2 was measured using EIS. The Bode modulus and phase plot were used to depict the impedance and phase within the 0.1 to 100 kHz frequency range (Figure 3a, b). The frequency response of impedance for Au-based I-ECG device showed decreased trend with increasing frequency (Figure 3a). From 0.3 Hz to 14 kHz, the impedance was several hundred kΩ. We measured the electrochemical impedance of electrodes at 1 Hz, which is close to a normal human heart rate.[22] The average impedance of the electrodes was 721.34 kΩ with standard deviation of

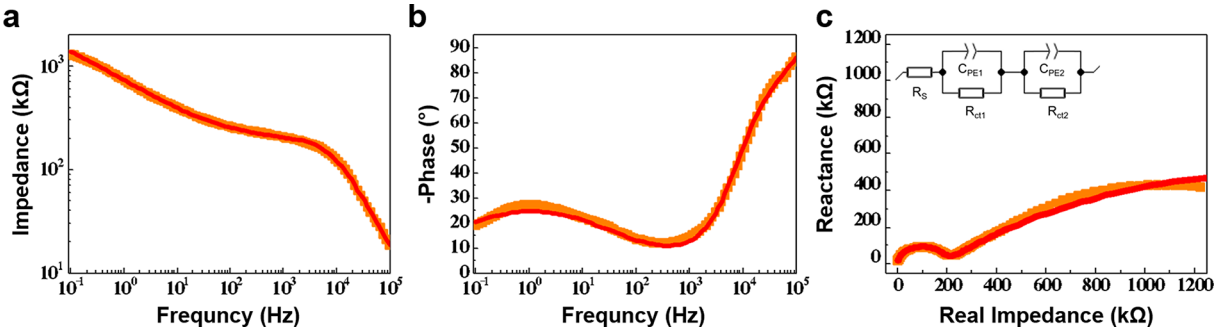

Figure 3. (a) Bode modulus, (b) Bode phase, and (c) Nyquist plot measurement data with fitted model of equivalent circuit (inset) under normal saline (0.9% w/v NaCl) solution.

DOI: 10.1021/acsbiomaterials.9b01102
ACS Biomater. Sci. Eng. 2020, 6, 2652−2658

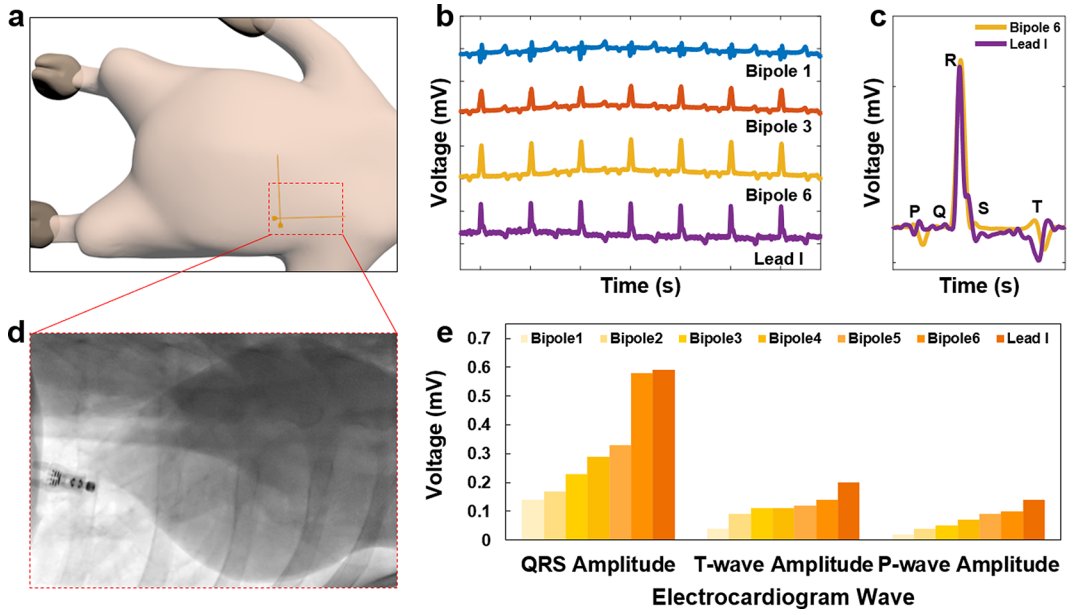

Figure 4. (a) In vivo scheme of vertically and horizontally implanted I-ECG device in the precordial subcutaneous space of a swine model. (b) Fluoroscopy. (c) Sinus rhythm signal detected at the closest (bipole 1), medial (bipole 3), and farthest (bipole 6) spacing between bipolar electrodes of vertical I-ECG device, compared to conventional surface ECG. (d) Expanded ECG signals of sinus signal (tick scale: *x*-axis 0.5 s, *y*-axis 0.5 mV). (e) Bar chart demonstrating the relationship between lead I of surface ECG and each bipole of I-ECG at the P, QRS, and T wave amplitudes.

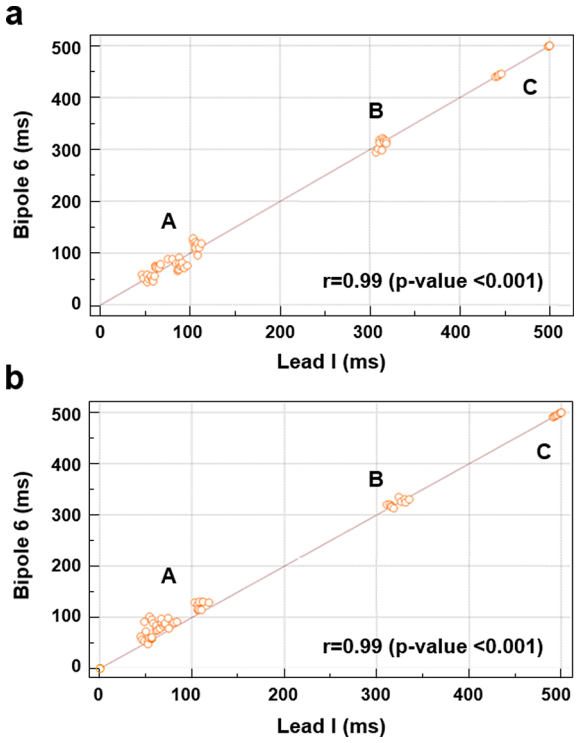

Figure 5. (A) Scatter plot of the P-, QRS-, and T-wave durations, (B) QT interval, (C) RR interval calculated on the basis of lead I and bipole 6 using a (a) horizontal and (b) vertical I-ECG device.

0.74 kΩ for electrodes (n = 7). The range of the impedance at 1 Hz for commercial Ag/AgCl 3 M ECG electrodes has a number of hundred kΩ to MΩ.[23,24] Compared with the gold standard commercial ECG, the I-ECG device provides an appropriate interface between electrode and subcutaneous skin to record the ECG signal. The phase shift has resistive characteristics (phase = 0°), with $\theta_{max} = -27°$ at 1 Hz, at the range up to ∼1 kHz and becomes more capacitive (phase = −90°) (Figure 3b). The Nyquist plot of Au-based ECG with fitting and a modeled equivalent circuit (inset) was used to study its charge carrying mechanism (Figure 3c). The circuit model includes a solution resistance (R_s), constant phase element impedance (C_{PE1}, C_{PE2}), and charge transfer resistance (R_{CT1}, R_{CT2}). The Nyquist plot exhibits two charge-transfer resistance (about R_{CT1} = 183 kΩ, R_{CT2} = 2687 kΩ) values, which can be estimated from each semicircle diameter, obtained by fitting with an equivalent circuit. The constant phase element is the behavior of an imperfect double-layer capacitor, where an ideal capacitor is n = 1.

$$C_{PE}(w) = \frac{1}{Q(jw)^n}$$

The C_{PE1} and C_{PE2} parameters of the equivalent circuit model are 0.17 nS s^1 and 0.63 μS $s^{0.44}$, respectively.

3.2. Device Implantation. Three I-ECG devices were tested for ECG detection in one animal during two separate experiments. In the first experiment two devices were tested. The first device was implanted vertically (parallel to the sternum) and the other was placed horizontally (perpendicular to the sternum) (Figure 4a). Simultaneous ECG tracings were recorded from the two devices. In the second experiment only one device was tested for ECG detection and was placed perpendicular to the sternum. We had a 100% success rate with device implantation as planned using the technique outlined in the procedure section. The needle was easily inserted and tunneled through the planned 0.5 cm incision with very little to no bleeding, hematoma, or significant ecchymosis (Figure 2). The small nature of the device required very gentle handling, but otherwise, the device was placed and the needle was retracted with no complications (Figure 2). Once the needle was retracted, the device flexibility allowed it to follow the natural contour of animal's chest while maintaining its

DOI: 10.1021/acsbiomaterials.9b01102
ACS Biomater. Sci. Eng. 2020, 6, 2652−2658

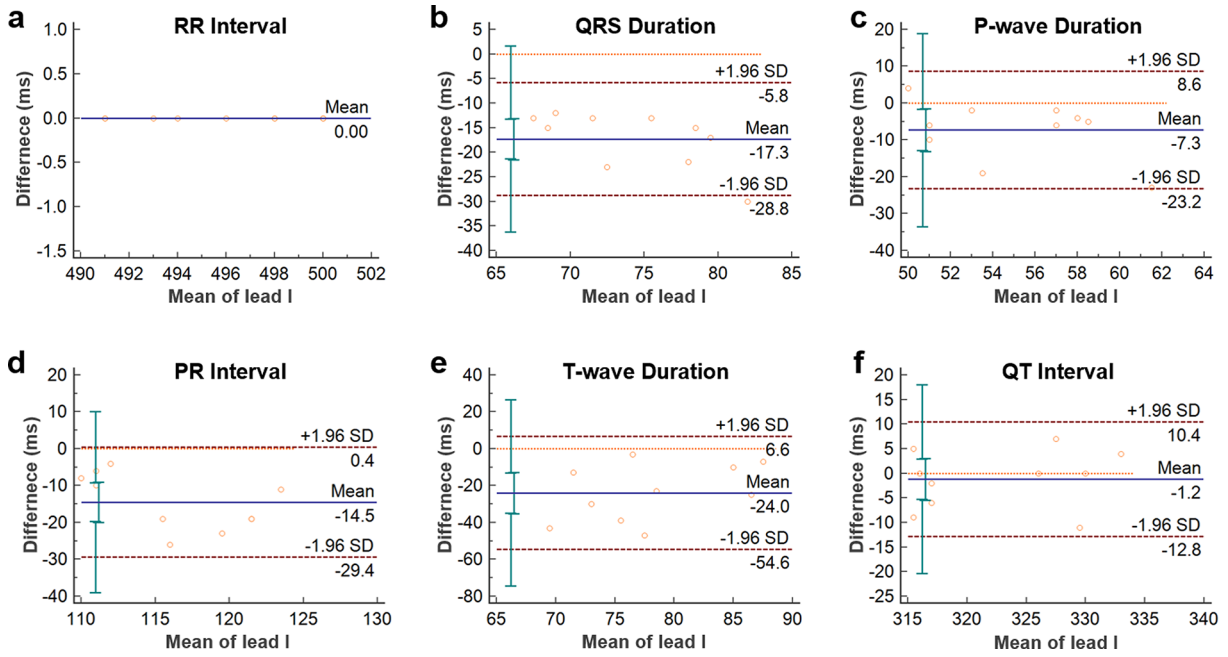

Figure 6. Bland–Altman plots showing the relationship between the mean of lead I and the differences measured by bipole 6 from I-ECG in (a) RR interval, (b) QRS duration, (c) P-wave duration, (d) PR interval, (f) T-wave duration, and (e) QT interval in sinus rhythm using vertical I-ECG device.

intended position even after manual compression of the skin over the device. The PI carrier successfully served as the supporting structure during the implantation procedure. The PVA dissolved as expected and the PI carrier was removed without complication, thus leaving the I-ECG device in place in 100% of tests on direct visualization. Because of the small thickness of the device (~15 μm-thick PI layers and 500 nm-thick metal layers (Ti/Cu/Au)) it was almost invisible on fluoroscopy image, whereas the externalized cable was clearly visible (Figure 4b).

The device was not left long-term in the animal with this protocol. However, after device extraction following the first experiment, there were no complications observed including any bleeding, hematomas, or infection. After 8 days, the animal was brought back to the procedure room for the second experiment. The site of previous device implantation did not show any evidence of complications and the second experiment was carried out successfully. The animal was sacrificed after the second experiment.

3.3. In Vivo Cardiac Signal. We were able to acquire ECG signals using all three I-ECG devices in our in vivo experiments (Figure 4). Using the proximal most electrode as reference, six bipolar signals were recorded from the first device that was placed vertically and horizontally (Figure 4a). One bipole failed in each of the horizontal devices because of high frequency noise and thus were excluded from the analysis. Bipolar signals were even obtained using one electrode from each device when implanted simultaneously during the first experiment (data not shown). Figure 4c shows sinus rhythm recorded by the closest (bipole 1), medial (bipole 3), and farthest (bipole 6) spacing of the vertical I-ECG device, compared with the surface ECG (lead I). In a sinus rhythm, traditional ECG signals such as the P, QRS, and T waves that were detected by any spacing of I-ECG device, are easily discernible. However, the morphology of the acquired ECG signal from the I-ECG device was dependent on the spacing between bipolar electrodes. Specifically, the amplitudes of the P, QRS, and T wave signals showed a strong correlation with electrode spacing (Figure 4c–e and Table S1). Therefore, the wider-spaced bipole resulted in a larger amplitude across all waves (P, QRS, and T). The largest bipole (bipole 6) was most reliable in identifying waves and measuring intervals (Figure 4d). The ease of wave detection allowed us to measure important physiologic parameters including PR, RR, and QT intervals.

Compared to surface ECG, and regardless of device position, bipole 6 showed excellent correlation of P, QRS, and T-wave durations, QT interval, and RR intervals, with a calculated correlation coefficient for horizontally and vertically placed devices of $r = 0.99$ ($p < 0.001$) as shown in Figure 5. The limits of agreement between bipole 6 and lead I from the Bland–Altman plots were ±30 ms for the QT interval, and ±0 ms for the RR interval. The relatively small ranges of the limits of agreement on Bland–Altman plots, compared to the measured parameter, suggests their clinical utility for measuring rate, rhythm, and QT intervals when placed in the vertical position (Figure 6). The same applies for PR interval, QRS-, P-, and T-wave durations from which clinicians can infer rhythm and origin of electrical impulse.

Pacing electrograms were reliably detected using all working electrodes on all devices. The device was able to detect the rate and rhythm reliably in sinus rhythm; however, the morphology was difficult to discern as compared to surface ECG (Figure S4a, b). Depending on the location of pacing, the P and T waves could not be accurately measured because of the pacing artifact. During ventricular pacing, there was an obvious change in QRS morphology compared to the sinus rhythm on the device. On qualitative analysis, there were excellent correlations of QRS durations and heart rates between the surface ECG and I-ECG in ventricular pacing. The I-ECG was able to detect arrhythmias such as PVCs, nonsustained

DOI: 10.1021/acsbiomaterials.9b01102
ACS Biomater. Sci. Eng. 2020, 6, 2652–2658

ventricular tachycardia, and ventricular fibrillation (not shown).

4. DISCUSSION

In this study, we demonstrated a novel flexible microelectrode-based injectable device to detect ECG signals. We also demonstrated the feasibility of device insertion in a swine model. Finally, we showed the suitability of the high-density channel microelectrode array study the dependency of different spacing between bipolar electrodes. Our novel device was able to record ECG signals in sinus rhythm and simulated arrhythmias (atrial and ventricular pacing). We demonstrated excellent correlation between the P, R, and T wave amplitudes with distance of bipoles. In other words, the bipole spacing affects the ECG amplitude, with wider spaced bipoles giving the best ECG. Thus, using the largest spacing of electrode bipole proved to be interchangeable with surface ECG when compared to lead I for detection of the RR intervals (used to determine rhythm and rate) in addition to QT durations in sinus rhythm based on the Bland–Altman plots.

In future iterations, we aim to improve the connectivity of our device to allow for wireless communication, which has the potential to significantly impact the current medical practice for ambulatory ECG monitoring and during electrophysiology procedures. The small size and ease of insertion of our device may allow it to be easily implanted in a primary care setting by general practitioners using surface anatomic landmarks, thus improving access to care and reduce costs. Moreover, these same factors can potentially be more tolerated and stay in position much longer than conventional devices and permit unique applications such as long-term rhythm monitoring with machine learning to predict the onset of arrhythmias or myocardial infarction.

ASSOCIATED CONTENT

Supporting Information

The Supporting Information is available free of charge on the ACS Publications website at DOI: 10.1021/acsbiomaterials.9b01102.

Schematic diagram of the fabrication process for the device; exploded side and top view of the device; schematic illustration to demonstrate the working principles of the procedure; in vivo simulated arrhythmia signals detected from the I-ECG; ECG parameters in sinus rhythm based on electrodes used to detect the signals (PDF)

Movie S1, operation of the implantation process (MP4)

AUTHOR INFORMATION

Corresponding Authors

*Email: friedman.paul@mayo.edu (P.A.F.).
*Email: mazq@engr.wisc.edu (Z.M.).

ORCID

Jihye Bong: 0000-0003-1970-3948
Sang June Cho: 0000-0002-7784-2498
Juhwan Lee: 0000-0002-1082-6290
Zhenqiang Ma: 0000-0001-9214-1342

Notes

The authors declare no competing financial interest.

ACKNOWLEDGMENTS

This work was partly supported by ARO under Grant W911NF-14-1-0652. The program manager is Dr. James F. Harvey. This research was also carried out with the support of internal funds from Mayo Clinic.

REFERENCES

(1) Narayan, S. M.; Wang, P. J.; Daubert, J. P. New Concepts in Sudden Cardiac Arrest to Address an Intractable Epidemic: JACC State-of-the-Art Review. *J. Am. Coll. Cardiol.* **2019**, *73* (1), 70–88.

(2) Solbiati, M.; Casazza, G.; Dipaola, F.; Barbic, F.; Caldato, M.; Montano, N.; Furlan, R.; Sheldon, R. S.; Costantino, G. The Diagnostic Yield of Implantable Loop Recorders in Unexplained Syncope: A Systematic Review and Meta-Analysis. *Int. J. Cardiol.* **2017**, *231*, 170–176.

(3) Ziegler, P. D.; Rogers, J. D.; Ferreira, S. W.; Nichols, A. J.; Richards, M.; Koehler, J. L.; Sarkar, S. Long-Term Detection of Atrial Fibrillation with Insertable Cardiac Monitors in a Real-World Cryptogenic Stroke Population. *Int. J. Cardiol.* **2017**, *244*, 175–179.

(4) Yasin, O. Z.; Vaidya, V. R.; Chacko, S. R.; Asirvatham, S. J. Inappropriate Sinus Tachycardia: Current Challenges and Future Directions. *J. Innov. Card. Rhythm Manag.* **2018**, *9*, 3239–3243.

(5) Brignole, M.; Bellardine Black, C. L.; Thomsen, P. E. B.; Sutton, R.; Moya, A.; Stadler, R. W.; Cao, J.; Messier, M.; Huikuri, H. V. Improved Arrhythmia Detection in Implantable Loop Recorders. *J. Cardiovasc. Electrophysiol.* **2008**, *19* (9), 928–934.

(6) Shen, W.-K.; Sheldon, R. S.; Benditt, D. G.; Cohen, M. I.; Forman, D. E.; Goldberger, Z. D.; Grubb, B. P.; Hamdan, M. H.; Krahn, A. D.; Link, M. S.; Olshansky, B.; Raj, S. R.; Sandhu, R. K.; Sorajja, D.; Sun, B. C.; Yancy, C. W. 2017 ACC/AHA/HRS Guideline for the Evaluation and Management of Patients With Syncope: Executive Summary. *Circulation* **2017**, *136* (5), e25–e59.

(7) Zehender, M.; Meinertz, T.; Keul, J.; Just, H. ECG Variants and Cardiac Arrhythmias in Athletes: Clinical Relevance and Prognostic Importance. *Am. Heart J.* **1990**, *119* (6), 1378–1391.

(8) Steinberg, J. S.; Varma, N.; Cygankiewicz, I.; Aziz, P.; Balsam, P.; Baranchuk, A.; Cantillon, D. J.; Dilaveris, P.; Dubner, S. J.; El-Sherif, N.; Krol, J.; Kurpesa, M.; La Rovere, M. T.; Lobodzinski, S. S.; Locati, E. T.; Mittal, S.; Olshansky, B.; Piotrowicz, E.; Saxon, L.; Stone, P. H.; Tereshchenko, L.; Turitto, G.; Wimmer, N. J.; Verrier, R. L.; Zareba, W.; Piotrowicz, R. 2017 ISHNE-HRS Expert Consensus Statement on Ambulatory ECG and External Cardiac Monitoring/Telemetry. *Heart Rhythm* **2017**, *14* (7), e55–e96.

(9) Liu, Y.; Norton, J. J. S.; Qazi, R.; Zou, Z.; Ammann, K. R.; Liu, H.; Yan, L.; Tran, P. L.; Jang, K.-I.; Lee, J. W.; Zhang, D.; Kilian, K. A.; Jung, S. H.; Bretl, T.; Xiao, J.; Slepian, M. J.; Huang, Y.; Jeong, J.-W.; Rogers, J. A. Epidermal Mechano-Acoustic Sensing Electronics for Cardiovascular Diagnostics and Human-Machine Interfaces. *Science Advances* **2016**, *2* (11), No. e1601185.

(10) Lee, S. P.; Ha, G.; Wright, D. E.; Ma, Y.; Sen-Gupta, E.; Haubrich, N. R.; Branche, P. C.; Li, W.; Huppert, G. L.; Johnson, M.; Mutlu, H. B.; Li, K.; Sheth, N.; Wright, J. A.; Huang, Y.; Mansour, M.; Rogers, J. A.; Ghaffari, R. Highly Flexible, Wearable, and Disposable Cardiac Biosensors for Remote and Ambulatory Monitoring. *NPJ Digital Med.* **2018**, *1* (1), 2.

(11) Fang, H.; Yu, K. J.; Gloschat, C.; Yang, Z.; Song, E.; Chiang, C.-H.; Zhao, J.; Won, S. M.; Xu, S.; Trumpis, M.; Zhong, Y.; Song, E.; Han, S. W.; Xue, Y.; Xu, D.; Cauwenberghs, G.; Kay, M.; Huang, Y.; Viventi, J.; Efimov, I. R.; Rogers, J. A. Capacitively Coupled Arrays of Multiplexed Flexible Silicon Transistors for Long-Term Cardiac Electrophysiology. *Nature Biomedical Engineering* **2017**, *1* (3), 0038.

(12) Lee, J.-H.; Seo, D.-W. Development of ECG Monitoring System and Implantable Device with Wireless Charging. *Micromachines* **2019**, *10* (1), 38.

(13) Bong, J.; Attia, Z. I.; Vaidya, V. R.; Jung, Y. H.; Padmanabhan, D.; Lee, J.; Kim, H.; Ladewig, D. J.; Noseworthy, P. A.; Asirvatham, S. J.; Park, D.-W.; Friedman, P. A.; Ma, Z. Radiolucent Implantable

DOI: 10.1021/acsbiomaterials.9b01102
ACS Biomater. Sci. Eng. 2020, 6, 2652–2658

Electrocardiographic Monitoring Device Based on Graphene. *Carbon* **2019**, *152*, 946−953.
(14) Sarkar, S.; Ritscher, D.; Mehra, R. A Detector for a Chronic Implantable Atrial Tachyarrhythmia Monitor. *IEEE Trans. Biomed. Eng.* **2008**, *55* (3), 1219−1224.
(15) Song, Z.; Jenkins, J.; Burke, M.; Arzbaecher, R. The Feasibility of ST-Segment Monitoring with a Subcutaneous Device. *J. Electrocardiol.* **2004**, *37*, 174−179.
(16) Gunda, S.; Reddy, Y. M.; Pillarisetti, J.; Koripalli, S.; Jeffery, C.; Swope, J.; Atkins, D.; Bommana, S.; Emert, M. P.; Pimentel, R.; Dendi, R.; Berenbom, L. D.; DiBiase, L.; Natale, A.; Lakkireddy, D. Initial Real World Experience with a Novel Insertable (Reveal LinQ™@Medtronic) Compared to the Conventional (Reveal XT™@Medtronic) Implantable Loop Recorder at a Tertiary Care Center — Points to Ponder! *Int. J. Cardiol.* **2015**, *191*, 58−63.
(17) Preminger, M. W.; Musat, D. L.; Sichrovsky, T.; Bhatt, A. G.; Mittal, S. Migration of an Implantable Loop Recorder into the Pleural Space. *HeartRhythm Case Rep* **2017**, *3* (11), 539−541.
(18) Schuhmann, T. G.; Zhou, T.; Hong, G.; Lee, J. M.; Fu, T.-M.; Park, H.-G.; Lieber, C. M. Syringe-Injectable Mesh Electronics for Stable Chronic Rodent Electrophysiology. *J. Visualized Exp.* **2018**, *137*, No. e58003.
(19) Baker, M. I.; Walsh, S. P.; Schwartz, Z.; Boyan, B. D. A Review of Polyvinyl Alcohol and Its Uses in Cartilage and Orthopedic Applications. *J. Biomed. Mater. Res., Part B* **2012**, *100B* (5), 1451−1457.
(20) Qiu, K.; Netravali, A. N. A Composting Study of Membrane-Like Polyvinyl Alcohol Based Resins and Nanocomposites. *J. Polym. Environ.* **2013**, *21* (3), 658−674.
(21) Cogan, S. F. Neural Stimulation and Recording Electrodes. *Annu. Rev. Biomed. Eng.* **2008**, *10* (1), 275−309.
(22) Lou, C.; Li, R.; Li, Z.; Liang, T.; Wei, Z.; Run, M.; Yan, X.; Liu, X. Flexible Graphene Electrodes for Prolonged Dynamic ECG Monitoring. *Sensors* **2016**, *16* (11), 1833.
(23) Baek, J.-Y.; An, J.-H.; Choi, J.-M.; Park, K.-S.; Lee, S.-H. Flexible Polymeric Dry Electrodes for the Long-Term Monitoring of ECG. *Sens. Actuators, A* **2008**, *143* (2), 423−429.
(24) Castrillón, R.; Pérez, J. J.; Andrade-Caicedo, H. Electrical Performance of PEDOT:PSS-Based Textile Electrodes for Wearable ECG Monitoring: A Comparative Study. *BioMed. Eng. OnLine* **2018**, *17* (1), 38.

DOI: 10.1021/acsbiomaterials.9b01102
ACS Biomater. Sci. Eng. 2020, 6, 2652−2658